Ultrasensitive search for long-lived superheavy nuclides in the mass range $A = 288$ to $A = 300$ in natural Pt, Pb, and Bi

F. Dellinger, O. Forstner, R. Golser, A. Priller, P. Steier, A. Wallner, G. Winkler, and W. Kutschera
University of Vienna, Faculty of Physics, Vienna Environmental Research Accelerator (VERA) Laboratory, Währinger Strasse 17, A-1090 Wien, Austria

(Received 17 March 2011; published 20 June 2011)

Theoretical models of superheavy elements (SHEs) predict a region of increased stability around the proton and neutron shell closures of $Z = 114$ and $N = 184$. Therefore a sensitive search for nuclides in the mass range from $A = 288$ to $A = 300$ was performed in natural platinum, lead, and bismuth, covering long-lived isotopes of Eka-Pt (Ds, $Z = 110$), Eka-Pb ($Z = 114$), and Eka-Bi ($Z = 115$). Measurements with accelerator mass spectrometry (AMS) at the Vienna Environmental Research Accelerator (VERA) established upper limits for these SHE isotopes in Pt, Pb, and Bi with abundances of $<2\times10^{-15}$, $<5\times10^{-14}$, and $<5\times10^{-13}$, respectively. These results complement earlier searches for SHEs with AMS at VERA in natural thorium and gold, which now amounts to a total number of 37 SHE nuclides having been explored with AMS. In none of our measurements was evidence found for the existence of SHEs in nature at the reported sensitivity level. Even though a few events were observed in the window for ^{293}Eka-Bi, a particularly strong pileup background did not allow a definite SHE isotope identification. The present result sets limits on nuclides around the center of the island of stability, essentially ruling out the existence of SHE nuclides with half-lives longer than ∼150 million years.

DOI: 10.1103/PhysRevC.83.065806 PACS number(s): 07.77.Ka, 07.77.Gx, 32.10.Bi, 82.80.Rt

I. INTRODUCTION

Ever since the intriguing possibility for the existence of an "island of stability" beyond the heaviest known nuclides was pointed out by nuclear theorists in the late 1960's [1–4], the search for their possible existence in nature was pursued with various methods [5,6]. When a half-life of 2.5 billion years was predicted for a nucleus with $Z = 110$ and $N = 184$ [7], possibly produced at stellar *r*-process conditions [8,9], an early search for such a nuclide was performed with accelerator mass spectrometry (AMS) in a natural platinum nugget [10]. In this experiment an upper limit of 1×10^{-11} for the abundance of this nuclide in Pt was established. It was assumed that the ^{294}110 nuclide would follow its chemical homologue Pt throughout the geochemical history on Earth, and, depending on its initial abundance when the solar system formed [8], one could deduce upper limits for its half-life in the 100-million-year range [10]. In a different approach, upper limits for the abundance of elements 107–110 in the Early Solar System were estimated from the ^{152}Sm abundance in the Santa Clara meteorite—assumed to be due to fission from superheavy elements (SHEs) [11]. For element 110, an upper limit of 3.4×10^{-5} relative to ^{238}U was estimated.

Some radionuclides live long enough to have survived since the solar system formed ∼4.6 billion years ago. Among them, ^{238}U ($t_{1/2} = 4.47\times10^{9}$ yr), ^{235}U ($t_{1/2} = 7.04\times10^{8}$ yr), and ^{232}Th ($t_{1/2} = 1.41\times10^{10}$ yr) are well known. The existence of the much shorter-lived ^{244}Pu ($t_{1/2} = 8.1\times10^{7}$ yr) in a rare-earth mineral has once been reported [12], but still awaits independent experimental verification. The slightly longer-lived ^{146}Sm ($t_{1/2} = 1.03\times10^{8}$ yr) has not yet been observed in nature, but AMS methods for a sensitive detection of this radionuclide are under development [13,14]. There are no radionuclides known with half-lives between 100 and 700 million years. From Table I it can be seen that the abundance of radionuclides with half-lives shorter than ∼200 million years is dramatically reduced.

If one assumes a production ratio of SHEs with respect to the investigated materials in *r*-process nucleosynthesis in the range of 10^{-2}–10^{-5} [8,9,15], and no further separation from the host element, then one might be able to detect SHEs with half-lives longer that ∼150 million years. Admittedly, this is a long shot, and some loopholes may still exist, but AMS allows one to probe into this realm with an unprecedented sensitivity. Besides measuring low abundances, the AMS search for a particular nuclide accepts a whole chain of neigboring isobars (i.e., also neighboring elements), because their mass differences are well within the mass acceptance of the AMS setup. Including isobars for such a search into the unkown is clearly advantageous, considering that the prediction of the elemental properties of SHEs is somewhat uncertain.

Since the early AMS search for ^{294}110 in platinum [10], the AMS technique has advanced considerably, allowing one to lower the abundance limits by several orders of magnitude [16–18]. The present work extends these ultrasensitive searches for SHE nuclides to natural platinum, lead, and bismuth. In particular, the mass range from $A = 288$ to 300 is investigated, covering part of the predicted island of stability around $Z = 114$ and $N = 184$ (Fig. 1). Although it was intended to cover the same mass range for isotopes of Eka-Hg (Cn, $Z = 112$) and Eka-Tl ($Z = 113$) as well, the lack of suitable material for the ion source and the difficulty to produce decent negative-ion beams prevented a meaningful search for these elements.

It should be pointed out that these AMS searches use tandem accelerators, thus depending on the ability of the SHE nuclides to form negative ions. It is known that most elements do form negative atomic ions [20,21], but some do not (e.g., N, Mg, Mn, Hg). Table II lists negative ions and electron affinities (EAs) for

TABLE I. Surviving fraction of radionuclides present today, after decay since the solar system formed (4.56 billion years ago).

Nuclide	Half-life (10^6 yr)	Fraction present today
^{238}U	4468	4.9×10^{-1}
^{235}U	704	1.1×10^{-2}
SHE	600	5.2×10^{-3}
SHE	500	1.8×10^{-3}
SHE	400	3.7×10^{-4}
SHE	300	2.3×10^{-5}
SHE	200	1.7×10^{-7}
SHE	150	7.1×10^{-10}
^{146}Sm	103	4.7×10^{-14}
^{244}Pu	81	1.1×10^{-17}

TABLE II. Electron affinities (EAs) of Pt, Au, Pb, PbF_3, and Bi, and of the corresponding eka elements.

Element/Compound	Z	Negative ion	EA (eV)	Ref.
Pt	78	Pt^-	2.13	[20]
Ds (Eka-Pt)	110	Ds^-	Not known	
Au	79	Au^-	2.31	[20]
Rg (Eka-Au)	111	Rg^-	1.56	[22]
Pb	82	Pb^-	0.37	[20]
(Eka-Pb)	114	$(Eka\text{-}Pb)^-$	0.0	[23]
			1.30	[24]
			−0.36	[24]
PbF_2	82	PbF_3^-	3.7	[25]
			3.49	[24]
$(Eka\text{-}Pb)F_2$	114	$(Eka\text{-}Pb)F_3^-$	5.18	[24]
			5.36	[24]
Bi	83	Bi^-	0.94	[20]
Eka-Bi	115	$(Eka\text{-}Bi)^-$	0.38	[26]

the elements and compounds used in the current investigation. For completeness, Au and roentgenium (Eka-Au) measured previously [18] is also included in the table.

Except for Ds isotopes, the relativistic calculation for EAs of the eka elements are also listed. For Eka-Pb relativistic calculations give different EAs, including values of 0.0, −0.36, and 1.30 eV. Low EAs may be expected from the low EAs of Pb (0.37 eV [20]). However, it is known that PbF_3^- ions form readily from PbF_2 samples in a cesium-beam sputter source [27], and high EAs of 3.7 eV [25] and 3.49 eV [24] are reported. Seth *et al.* [23] calculated that Eka-Pb also forms a stable compound with fluorine, $(Eka\text{-}Pb)F_2$. Relativistic calculations [24] for the EA of $(Eka\text{-}Pb)F_3^-$ give high values, indicating an efficient production of negative ions for this molecule. Therefore this form was chosen in the search for SHEs of Eka-Pb.

The AMS measurements were performed at the Vienna Environmental Research Accelerator (VERA), a facility for "all" isotopes [28]. In particular, VERA has been optimized to measure heavy radionuclides with utmost selectivity [27]. Figure 2 shows a schematic layout of VERA, indicating the multiple filtering process to select a SHE nuclide. This cleaned

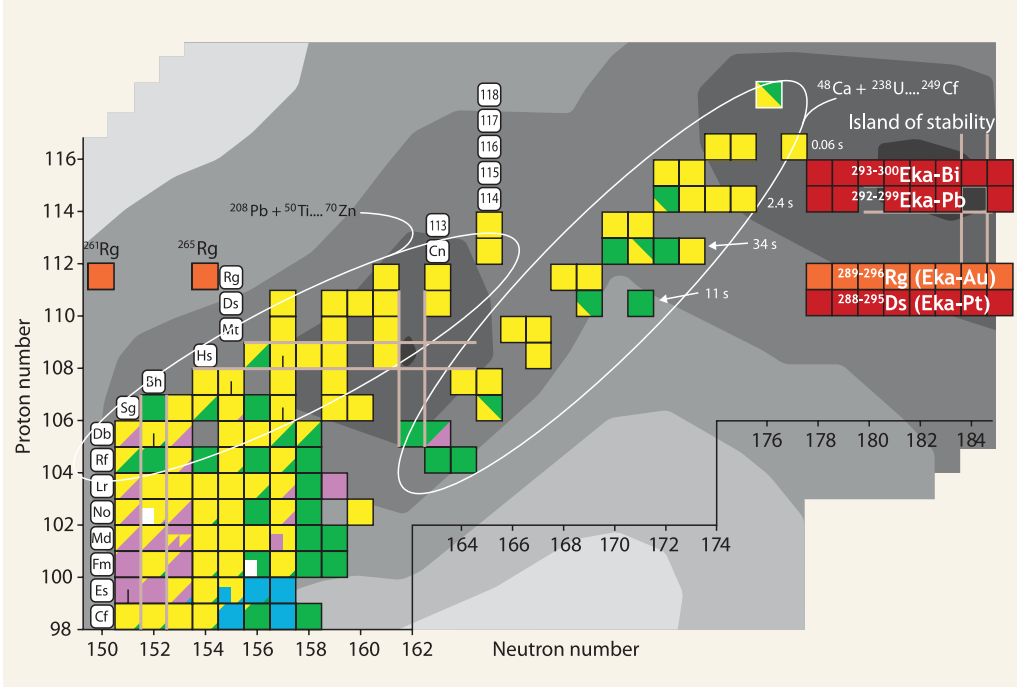

FIG. 1. (Color online) The figure depicts the upper end of the chart of nuclides, as shown in Ref. [19]. The various shades of gray indicate the calculated surface of the stability of nuclides (darker means more stable). The labels on the ellipses indicate the types of heavy-ion reactions that were used to produce the enclosed nuclides. The figure has been modified to include the SHE nuclides (orange boxes) investigated in our previous work (Rg isotopes [18]), and the ones from the present search (red boxes). The nuclides ^{294}Eka-Pb and ^{298}Eka-Pb could not be investigated because of an excessive background of interfering ions.

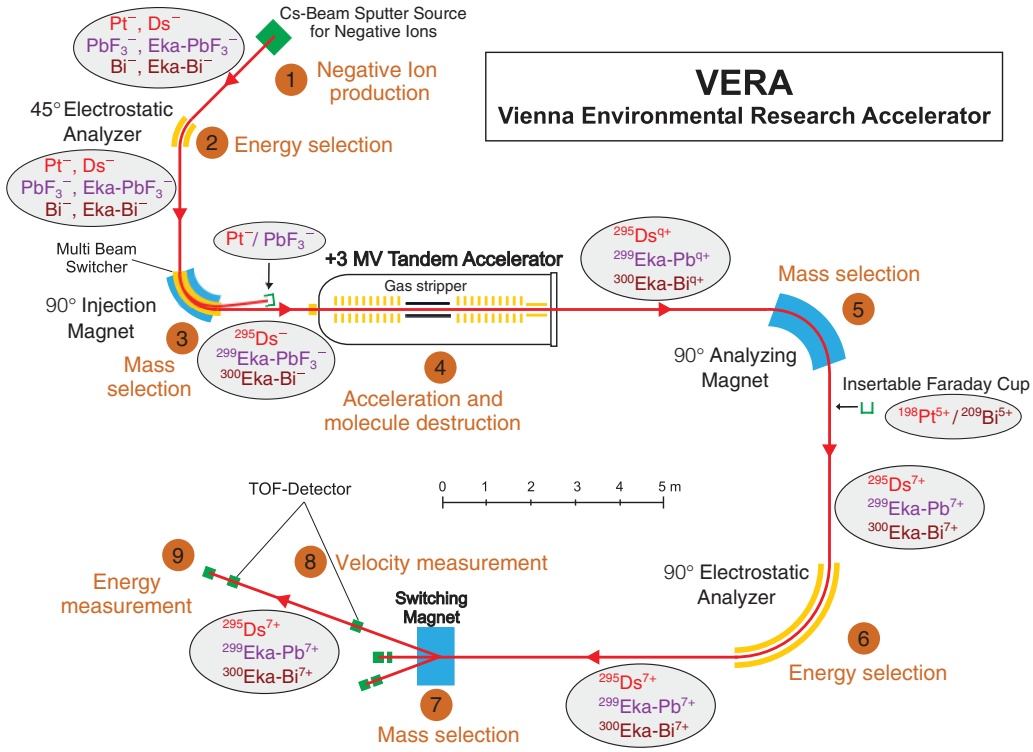

FIG. 2. (Color online) Schematic layout of the setup for the detection of SHE isotopes at VERA. The bubbles depict ions of the host elements at different stages of analysis, and the corresponding SHE ions. Only the respectively heaviest SHE isotopes are indicated. A ninefold filtering process is applied in our search for SHE isotopes: (1) negative-ion production (including background ions not indicated in the figure but used partly as reference ions; see text), (2) energy and charge selection, (3) momentum and charge selection (mass sensitive), (4) breakup of molecules in the gas (O_2)-stripping process, (5) momentum and charge selection, (6) energy and charge selection, (7) momentum and charge selection, (8) TOF (velocity) measurement, (9) residual energy measurement.

up the region of interest from any interfering background. However, in one case (^{293}Eka-Bi, see below) strong pileup was present from an intense background peak. A detailed analysis of this background was necessary to demonstrate that the observed events are most likely not from ^{293}Eka-Bi. It is important to note that this background occurred in spite of the highly selective system preceding the final energy detector. On the other hand, it is very important to guarantee the acceptance of the system for the species one is searching for. This aspect has been described in some length in Ref. [18], and will therefore not be repeated here.

In Sec. II we specify the sample materials and report on the sample preparation for the AMS measurements. In Sec. III we describe the tuning procedure of VERA for the various measurement setups, and in Sec. IV the results of our measurements are presented. Finally, in Sec. V we give a brief summary of our search for SHEs in natural materials at the VERA lab.

II. SAMPLE MATERIAL AND PREPARATION

It is well known that elements of similar chemical behavior are aligned in chemical groups in the Periodic Table (Fig. 3). The question as to whether the chemical resemblance also holds for the heaviest representatives of a respective group, where relativistic effects increase, is still unclear. When the chemical behavior cannot be exactly determined, one has to rely on theoretical predictions [22–24,26,32] or indications deduced from one-atom-at-a-time-chemistry experiments. Some of these recent experiments show [33–36] that the chemical properties of SHEs with Z from 104 to 118 may resemble those of the lighter homologues, however, exceptions from that trend are also known, especially for elements at the beginning of this series (see Ref. [33] and references therein).

Assuming that a SHE chemically resembles the sample (bulk) material, it may follow that material through physical and geochemical processes, thus increasing the chance to find it there, and not in materials of different chemical properties.

With the above arguments in mind, we focused on natural samples which are chemical homologues to the respective SHEs as the most promising materials for our experiments. In contrast to other (more simple) measurement techniques, AMS allows the measurement of chemically unpurified samples due to almost complete background suppression. Thus, three minerals were purchased on the Internet and further material was donated by the Department of Mineralogy and Petrography of the Natural History Museum Vienna (NHM). Table III lists some information on the sample material used in this study.

The best way to avoid an unintended separation of SHE atoms from the (chemically homologue) sample matrix is to avoid chemical preparation altogether. Concerning the search for long-lived Ds isotopes in natural Pt, this could be easily

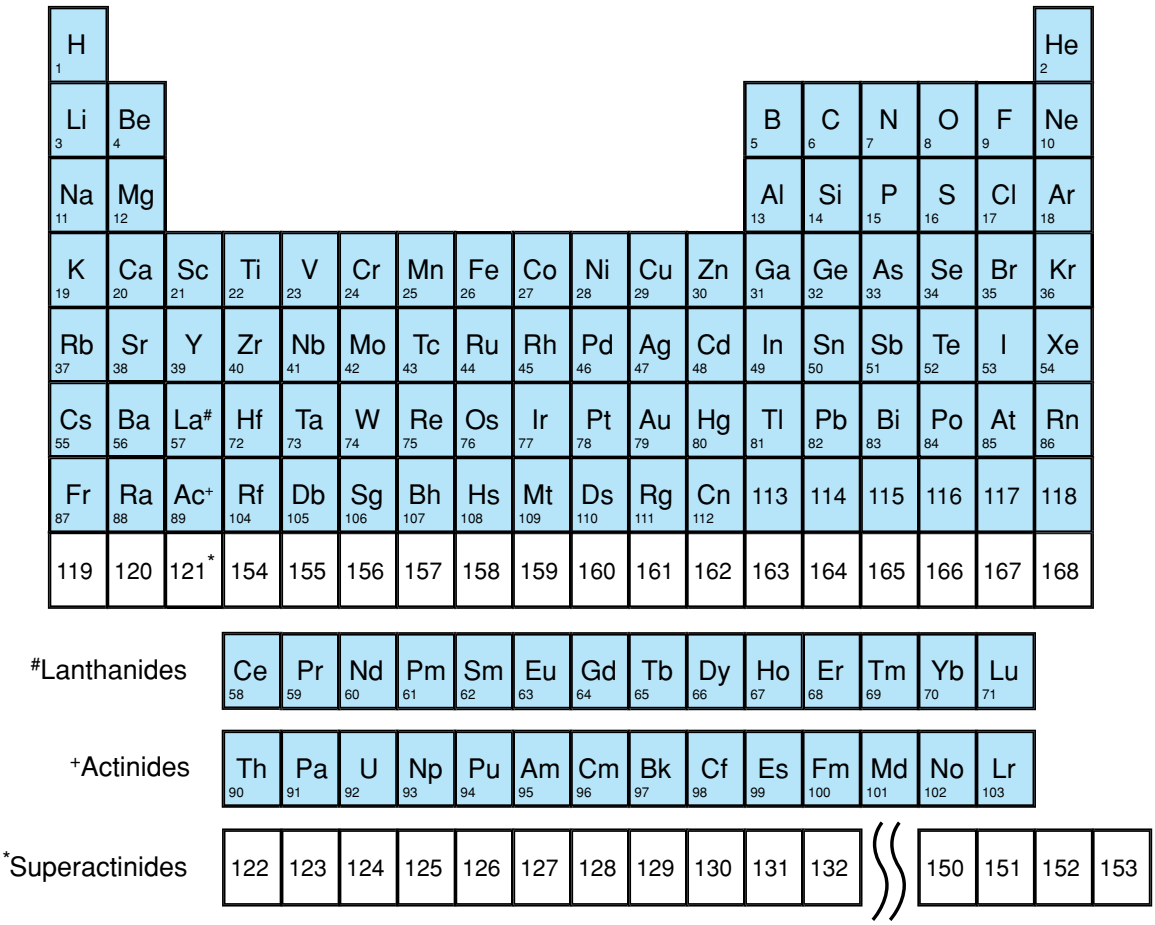

FIG. 3. (Color online) The Periodic Table of the elements. Numbers give the respective proton number of the element. The blue area shows the elements which are currently known. The white area shows a schematic extension of the Periodic Table as envisioned by Glenn Seaborg in 1969 [29,30]. It is interesting to note that at that time lawrencium ($_{103}$Lr) was the heaviest element known. Fourteen new elements, all the way up to the possible noble-gas-like Eka-Rn with $Z = 118$, have since been synthesized by heavy-ion reactions in various laboratories around the world [31].

fulfilled, since solid Pt (e.g., in the form of nuggets) forms prolific negative-ion beams [21]. Pieces of the sample material were directly pressed into the aluminum target holders of our multicathode source of negative ions by Cs sputtering (MC-SNICS) [37,38]. The sample material for the Eka-Bi beam time was prepared in a similarly plain way. Bismite (Bi_2O_3)—a claylike, yellowish deposit on a piece of rock weighing ∼650 g—was scraped off the rock with a wire brush and mixed with silver powder by weight in the ratio of ∼2:1. The mixture was then pressed into aluminum target holders.

However, for the Eka-Pb measurements chemical pretreatment had to be performed. Although natural galena (PbS) would readily form negative ions [21], it would also contaminate the ion source of VERA with ^{36}S, which is present in natural sulfur with an abundance of 0.02%, and would

TABLE III. Compilation of the natural samples used in our search for SHEs in platinum, lead, and bismuth minerals. The location and the total mass of the samples are listed. Concerning the largest platinum sample and the galena mineral, only a small fraction of the material was used up in our measurements.

Sample name	Material	Location	Sample mass
Pt-gcn	Gold-coated Pt nugget	Khabarovskiy Kray, Kondyor Massif, Russia	393 mg
Pt-NHM-1702	Pt nuggets	Ural Mountains, Russia	9 mg
Pt-NHM-2047	Pt nuggets	Brasilia	73 mg
Pt-NHM-2788	Pt nuggets	Chico, Colombia	23 mg
Gal	Galena (PbS)	Mibladen Mine, Upper Moulouya lead district, Morocco	122 g
Bis	Bismite (Bi_2O_3)	Schneeberg, Erzgebirge, Germany	150 mg (deposit)

therefore affect ongoing ^{36}Cl AMS measurements at the VERA lab. In previous measurements on ^{210}Pb [27], PbF_2 was found to be a suitable target material, with PbF_3^- to be the most intense lead fluoride current out of the source. Thus 4.2 g of PbS were ground to powder and dissolved in hot HNO_3. The solution was evaporated, the $Pb(NO_3)_2$ residue dissolved in double-distilled H_2O, and after centrifugation was evaporated again. The dissolution step in H_2O was repeated and the aquatic solution of $Pb(NO_3)_2$ was evaporated to 70 ml before it was mixed with 5 ml HF (24%) to precipitate PbF_2. Finally, the precipitation was centrifuged and dried at 90 °C overnight. Part of the material was mixed with aluminum powder in the ratio 1:1, whereas the rest was pressed directly into aluminum target> holders.

In addition to the natural samples some chemically processed target materials were included as sort of complementary target types in two measurements. For the Ds measurements, platinum wire supplied by Goodfellow (sample name Pt-gf) was investigated, whereas some targets with pure Bi powder (99.999% supplied by Alfa Aesar) were included in the Eka-Bi beam times.

III. TUNING THE AMS SYSTEM AND MEASUREMENT PROCEDURE AT VERA

The SHE measurement setups were established by using molecular pilot beams. Therefore, negatively charged molecules of almost the same mass as the SHE isotopes of interest were selected to tune the low-energy side of the AMS facility VERA (see Fig. 2). The singly charged negative molecules are accelerated to the tandem terminal gas stripper (typically at +3 MV), where they break up and a positively charged atomic ion with almost the same m/q ratio as the SHE isotopes sought for is used to tune the high-energy side of VERA.

Only the settings of the electric components of the AMS system are then scaled to the calculated values for the superheavy ion species, leaving the magnetic components unchanged, which guarantees reproducibility when switching between different setups in the measurement process (see below).

For all tuning materials a full mass scan of isotopologues (i.e., identical molecules that differ only in their isotopic composition) was performed to ensure that the correct mass peak is selected. Since all tuning molecules used in this study for SHE isotopes consisted of a (nearly) monoisotopic element plus two tellurium isotopes (see below), the pattern of the mass scan was similar to that of Te_2, shifted by the mass of the additional isotope.

Tuning with Te_2 was already used in our previous search for roentgenium isotopes in Au [18], because the heaviest mass peaks are separated by two atomic mass units, and therefore the automatic tuning algorithm AUTOMAX [39] is unlikely to be confused by an intense neighboring mass peak during the tuning process. In the high-mass region investigated in the current study this could lead to problems, since the relative difference between masses gradually decreases with increasing mass.

For tuning purposes, the following targets were prepared: (1) Al metal filings were mixed with tellurium powder in a volume ratio of ∼1:2 and pressed into Al target holders; (2) niobium telluride powder was pressed directly into Al target holders; and (3) vanadium filings were mixed with tellurium powder and pressed into Al target holders. In the search for superheavy Ds isotopes the negative molecular ion ^{27}Al^{126}Te^{130}Te$^-$ (m = 283) was used from (1) to tune the low-energy side of VERA for $^{288-295}$Ds$^-$, and after molecular breakup at the tandem terminal gas stripper the atomic fragment ^{126}Te^{3+} was used to set up the high-energy side for $^{288-295}$Ds^{7+}. In the search for superheavy Eka-Pb isotopes, targets of (2) were used and the low-energy side was tuned for ^{A}Eka-PbF_3^- (A = 292, 293, 295–297, 299) using a molecular pilot beam of ^{93}Nb^{128}Te^{130}Te$^-$ (m = 351), whereas the fragment ^{128}Te^{3+} allowed to tune the high-energy side for the ^{A}Eka-Pb^{7+}ions. In the Eka-Bi beam time, ^{51}V^{126}Te^{128}Te$^-$ (m = 305) was utilized from targets (3) to establish the low-energy setup for $^{293-300}$Eka-Bi$^-$ and ^{128}Te^{3+} to set up the high-energy side for $^{293-300}$Eka-Bi^{7+}.

The closer the m/q ratios of pilot ions match the ones of the SHE isotopes, the more accurate the scaling process can be applied. However, too close-lying m/q ratios may produce a stronger background in the measurement.

In recent AMS measurements of uranium and plutonium isotopes at VERA it was shown [40,41] that reliable scaling is possible for m/q ratios within a relative deviation of 2.5%.

Table IV compares the m/q ratio of tuning ions with the m/q ratio of the rare ions. It should be emphasized that all tuning ions deviate less than 2.5% in m/q ratios from the respective SHE ions.

The measurements were performed in beam times at different times (see below). A beam time is subdivided in a large number of runs on different targets of the same element. The measurement sequences within one run were typically

TABLE IV. Comparison of the m/q ratio of the tuning ions with the m/q ratio of the lightest and heaviest SHE ions.

High-energy tuning ion	m/q of tuning ion	SHE ion	m/q of SHE ion	$\Delta(m/q)/(m/q)$ (%)
^{126}Te^{3+}	42.00	^{288}Ds^{7+}	41.14	2.09
^{126}Te^{3+}	42.00	^{295}Ds^{7+}	42.14	−0.33
^{128}Te^{3+}	42.67	^{292}Eka-Pb^{7+}	41.71	2.30
^{128}Te^{3+}	42.67	^{299}Eka-Pb^{7+}	42.71	−0.09
^{128}Te^{3+}	42.67	^{293}Eka-Bi^{7+}	41.86	1.94
^{128}Te^{3+}	42.67	^{300}Eka-Bi^{7+}	42.86	−0.44

arranged in the following order: reference ion 1 (∼20 s) – reference ion 2 (∼20 s) – reference ion 3 (∼20 s) – SHE isotope 1 (∼200 s) – SHE isotope 2 (∼200 s) – SHE isotope 3 (∼200 s) – SHE isotope 4 (∼200 s). Hence the total time per run adds up to ∼1000 s, including the switching time between the setups. The purpose of measuring so-called reference ions is to monitor the stability of the components of the AMS system. Therefore, the tuning setup is scaled for the detection of ions with close-lying magnetic rigidity (e.g., $^{208}Pb^{5+}$ for $^{288}Ds^{7+}$, see Fig. 4). A moderate count rate of ∼100 Hz in the detection system would change significantly if an AMS-system component would accidentally drift away from its nominal setting.

In order to calculate atomic ratios from registered counts, currents for normalization of the count rate have to be measured. For the Ds beam time, both the Pt^- current in an offset Faraday cup on the low-energy side and the $^{198}Pt^{5+}$ current after the analyzing magnet on the high-energy side (see Fig. 2) were measured at the beginning and at the end of each run. A run consisted of the sequence mentioned above. Typical currents for Pt^- were in the 20–30 μA range and ∼80–160 enA (electrical nanoamps) for $^{198}Pt^{5+}$. For the Eka-Pb beam time, the PbF_3^- current output of the ion source was monitored quasipermanently in a low-energy offset Faraday cup. The voltage of the multibeam switcher at the injection magnet (see Fig. 2) was therefore altered for a duration of ∼3 ms every 0.2 s in such a way that PbF_3^- was injected into a low-energy offset Faraday cup, with typical currents of 1–2 μA for a new cathode (average currents of 900 nA were maintained for the first beam time, and 400 nA for the second beam time). In this case, a high-energy current for stable isotopes of Pb^{5+} ions was not measured. For the Eka-Bi beam time, $^{209}Bi^-$ measurements after the injection magnet were corrupted, and therefore only the high-energy current of $^{209}Bi^{5+}$ was measured after the analyzing magnet at the beginning and at the end of each run on the isotopes $^{297-300}$Eka-Bi^{7+}. The $^{209}Bi^{5+}$ currents were in the range of 10 enA.

A crucial quantity for calculating the final atom ratios is the transmission of the rare ions through the AMS system. The main constituents of that factor are the efficiency of the terminal stripping process to the respective charge state and the detector efficiency [Bragg and time-of-flight (TOF) detector]. The question of the unknown stripping efficiency for SHEs was already addressed by measuring the charge distributions of ^{197}Au and ^{238}U injected at the same velocity into the terminal gas stripper as the corresponding SHE isotopes, and extrapolating to the superheavy region [18]. For the current study we adopted a value of $\sim 1.5 \times 10^{-3}$ for the transmission from the injector (low-energy current) to the detector (registered counts), as determined in our previous search for SHEs [18].

At the detection system three signals from the incoming ions were recorded. Besides the pulse-height and the pulse-width signal of a Bragg-type ionization chamber, the TOF signals of a 2.8-m-long TOF section were measured. The combination of these three parameters allowed the effective suppression of pileup events in the evaluation process (see Fig. 7 in Ref. [18]).

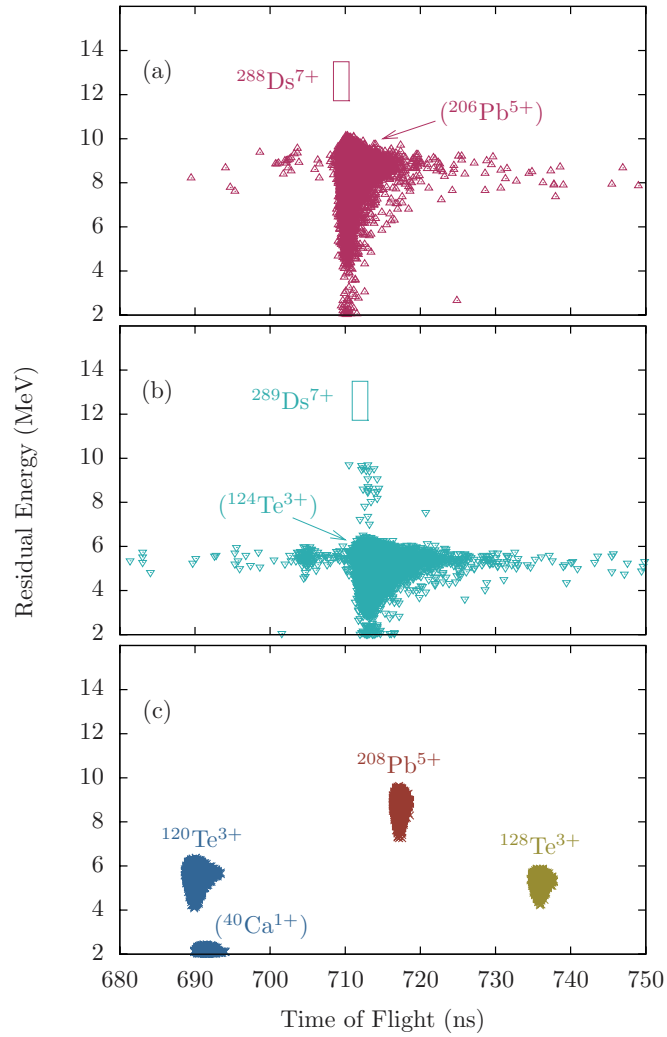

FIG. 4. (Color online) Spectra of residual energy (E_{res}) vs TOF recorded during the second beam time (a) with the AMS system tuned for the detection of $^{288}Ds^{7+}$ and (b) of $^{289}Ds^{7+}$. In (c) the individual spectra of the three reference ions ($^{120}Te^{3+}$, $^{128}Te^{3+}$, and $^{208}Pb^{5+}$) are plotted together (composite spectrum). To show the peak position of the reference ions clearly, only channels containing more than ten events are plotted in this spectrum (c). In contrast, all events are shown in (a) and (b). Isotope labels in brackets indicate the possible assignment of ions based on the TOF and residual energy signals for all three plots. In both spectra (a) and (b) the window for the superheavy ion species remained free of events. Whereas $^{206}Pb^{5+}$ is the main background constituent in the setup for $^{288}Ds^{7+}$, it is mainly $^{124}Te^{3+}$ which generates the background count rate in the $^{289}Ds^{7+}$ setup.

IV. RESULTS AND DISCUSSIONS

The Ds measurement consisted of three consecutive beam times. Before each period of data acquisition (lasting ∼12 h), the AMS system was (re-)tuned using the procedure described in Sec. III. To show the spectra in ascending order of mass number, the second beam time is described first.

A total of 35 runs were performed in the second beam time on August 13–14, 2009 to search for $^{288-291}Ds$ on the targets Pt-gf, Pt-gcn, Pt-NHM-2047, and Pt-NHM-2788. Figures 4

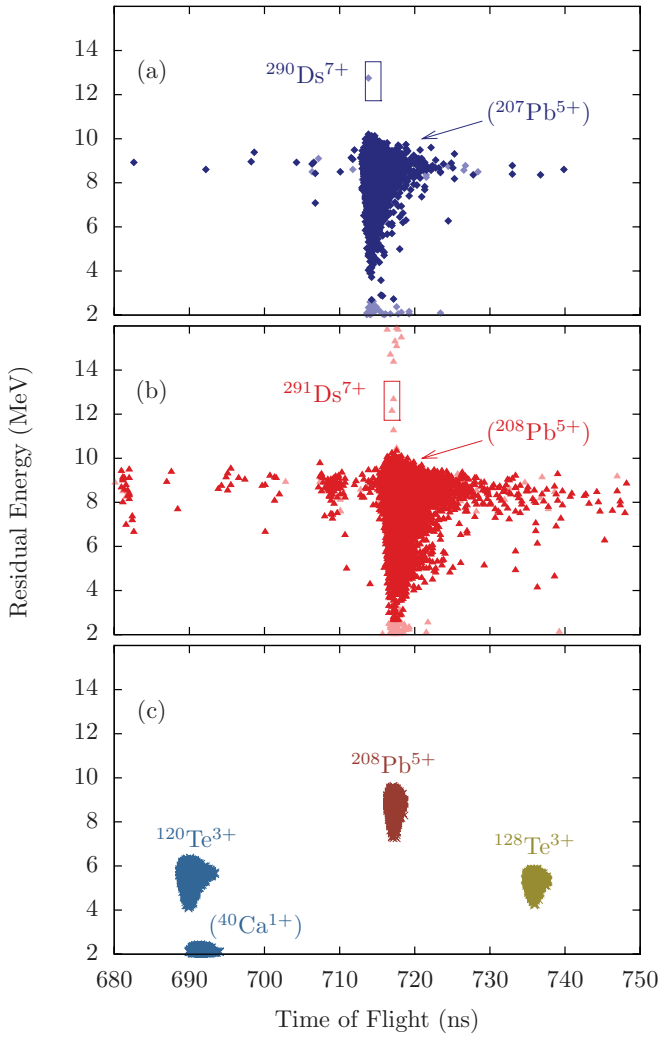

FIG. 5. (Color online) E_{res} vs TOF spectra for (a) ^{290}Ds^{7+}, (b) ^{291}Ds^{7+}, and (c) reference ions, plotted in the same way as described in the caption of Fig. 4. As main background components, ^{207}Pb^{5+} and ^{208}Pb^{5+} have been identified for the ^{290}Ds^{7+} and ^{291}Ds^{7+} setups, respectively. One event in the upper spectrum and two events in the lower have been detected within the windows of Ds. However, when the pulse-width criterion (see Fig. 7 in Ref. [18]) was applied, all events could be rejected (light colors in the plots).

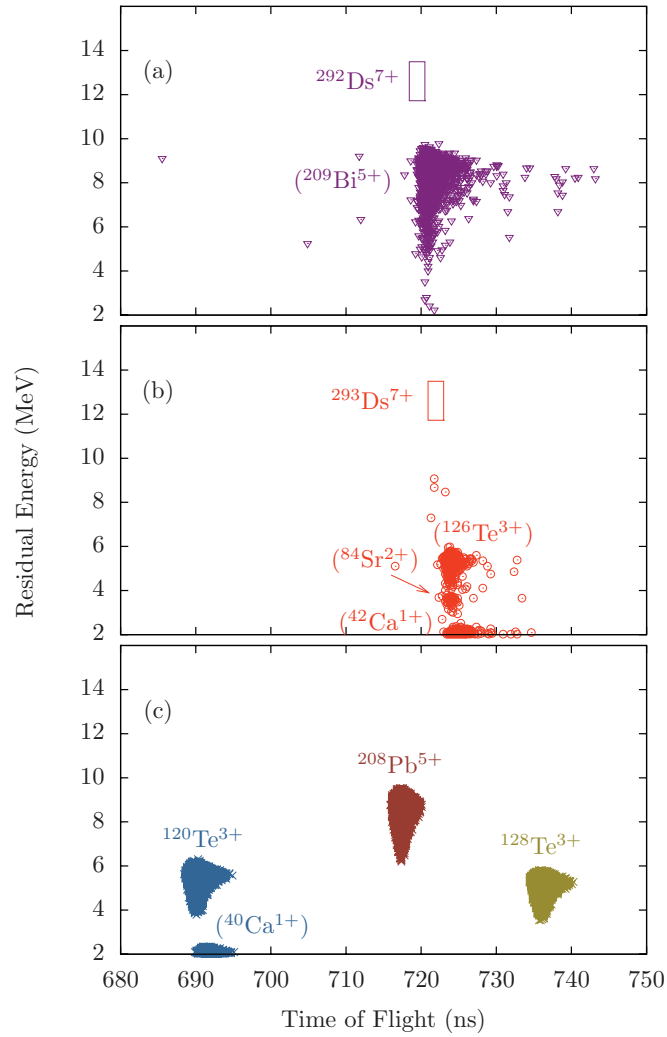

FIG. 6. (Color online) E_{res} vs TOF spectra for (a) ^{292}Ds^{7+}, (b) ^{293}Ds^{7+}, and (c) reference ions, plotted in the same way as described in the caption of Fig. 4. These spectra were accumulated in the first beam time (see the text). Both windows for the superheavy Ds isotopes remained free of events. In the setup for ^{292}Ds^{7+} a moderate background of ^{209}Bi^{5+} was detected, whereas ^{126}Te^{3+}, ^{84}Sr^{2+}, and ^{42}Ca^{1+} were seen in the spectrum for ^{293}Ds^{7+}.

and 5 show the residual energy (E_{res}, i.e., the residual energy of ions after passing the TOF pickup foils and the entrance window of the Bragg detector) versus TOF spectra of all runs of the second beam time. Identifiers in brackets indicate a possible assignment due to the position in the TOF vs E_{res} spectrum. The identifiers without brackets refer to ions which the AMS system was tuned for (i.e., reference ions and SHEs). In the spectra of the lightest Ds isotopes investigated, ^{288}Ds and ^{289}Ds (Fig. 4), no event could be found within the window, where these respective SHE isotopes would be expected. The two conspicuous background peaks of ^{206}Pb^{5+} and ^{124}Te^{3+} were observed in the setups for ^{288}Ds and ^{289}Ds, respectively. The spectrum of the ^{290}Ds^{7+} setup in Fig. 5 shows one detected event slightly above the middle of the window for ^{290}Ds^{7+}. However, this event had to be rejected (light color in the plot), since the pulse-width criterion was not fulfilled (see the explanation in Sec. IV of Ref. [18]).

In the spectrum of ^{291}Ds^{7+} [Fig. 5(b)] the intense peak of ^{208}Pb^{5+} most probably produced some pileup events [light symbols in Fig. 5(b)], also situated within the window of ^{291}Ds^{7+}. Since suppression of 5+ pileup events in a measurement setup for 7+ ions works very efficiently [18], both events could be identified as background and excluded.

In the first beam time on August 12–13, 2009, a total of 46 runs were performed to search for the isotopes $^{292-295}$Ds, on the same targets as in the second beam time. No event was detected within the windows for the superheavy isotopes $^{292-295}$Ds. The background count rates in those four setups were small enough that no significant amount of pileup events was created. In the setup for ^{292}Ds^{7+} [Fig. 6(a)] a considerable background peak of ^{209}Bi^{5+} could be identified,

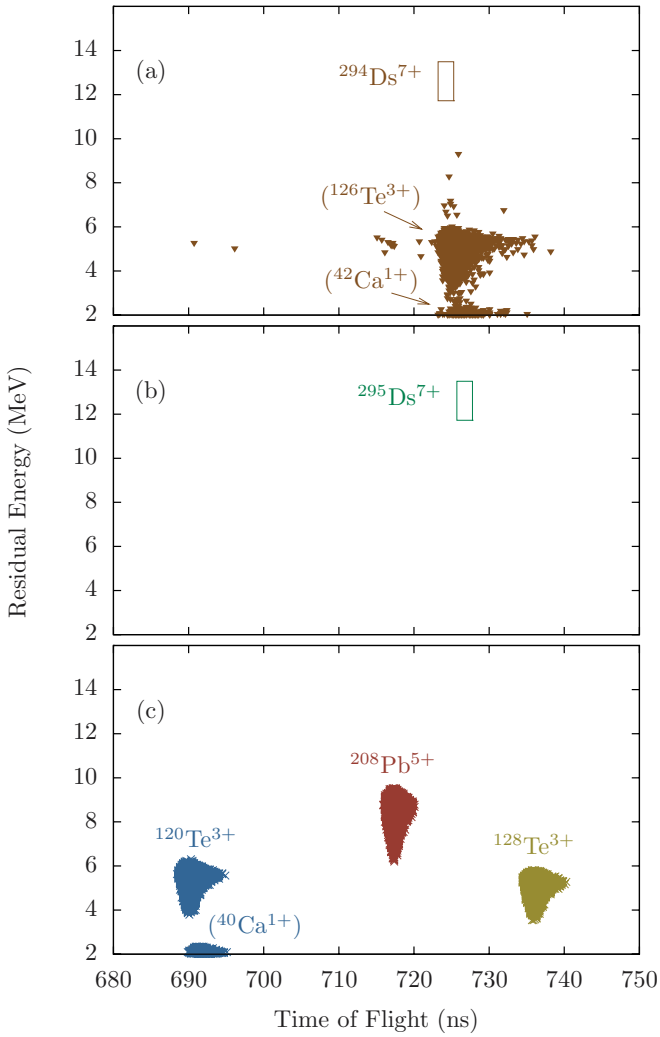

FIG. 7. (Color online) E_{res} vs TOF spectra for (a) ^{294}Ds^{7+}, (b) ^{295}Ds^{7+}, and (c) reference ions, plotted in the same way as described in the caption of Fig. 4. These spectra were recorded during the first beam time of the Ds measurement. Whereas spectrum (a) shows background peaks of ^{126}Te^{3+} and ^{42}Ca^{1+}, the spectrum for ^{295}Ds^{7+} (b) remains completely free of background events. However, in the third beam time, where the isotopes $^{292-295}$Ds^{7+} were remeasured, the spectrum for ^{295}Ds^{7+} contained ten background events of ^{169}Tm^{4+}.

whereas in the setup for ^{293}Ds^{7+} mainly the ions ^{126}Te^{3+}, ^{84}Sr^{2+}, and ^{42}Ca^{1+} were detected. Likewise in the ^{294}Ds^{7+} setup [Fig. 7(a)] ^{126}Te^{3+} and ^{42}Ca^{1+} constitute the main background. Interestingly, not a single background event was detected in the ^{295}Ds setup during this beam time. This low background was confirmed by a third beam time where only ten events of ^{169}Tm^{4+} were recorded for the ^{295}Ds setup within 32 runs.

In the third beam time on August 14–15, 2009 (32 runs) the isotopes $^{292-295}$Ds were remeasured. Additionally to the material used in the beam times before, the nugget from the Ural Mountains (Pt-NHM-1702) was included in this measurement. The spectra of this beam time appear to be very similar to those shown in Figs. 6 and 7, confirming the results of the first beam time.

In Table V the results of the three beam times on Pt targets are summarized. The upper limits in the last column are given assuming a Poisson distribution for detected events, in particular, considering the probability of measuring zero events (if no events have been detected), and calculated at a 90% confidence level so that the real abundances are not greater than the given values (see, e.g., Feldman *et al.* [42]). All calculated ratios are in the lower 10^{-15} range.

The second element investigated for the possible existence of a superheavy element was lead. Two consecutive beam times on April 11–12, 2009 (45 runs) and April, 12–13, 2009 (70 runs) were performed on PbF_2 targets to search for ^{A}Eka-Pb (A = 292, 293, 295, 296, 297, 299). Unfortunately, an intense background of ^{126}Te^{3+} and ^{128}Te^{3+} (>5000 counts per second in the Bragg detector) in the setups for ^{294}Eka-Pb^{7+} and ^{298}Eka-Pb^{7+} made a search for these isotopes impossible. Instead, the search for the heaviest Eka-Pb isotopes of our study, ^{297}Eka-Pb^{7+} and ^{299}Eka-Pb^{7+}, has been intensified by remeasuring those isotopes in both beam times.

Generally, the second beam time suffered from smaller low-energy PbF_3^- currents (average currents of ∼350 nA instead of 850 nA for the first beam time), since the fast sputtering of lead fluoride targets significantly decreased the current output after the first beam time.

In Fig. 8 the E_{res} vs TOF composite spectra of the ^{292}Eka-Pb^{7+} and ^{293}Eka-Pb^{7+} setups measured in the second beam time are plotted. In both setups the predominant background ions were ^{125}Te^{3+}, ^{126}Te^{3+}, ^{208}Pb^{5+}, and ^{209}Bi^{5+}, at different

TABLE V. Results of the search for Ds isotopes in Pt samples.

Rare isotope	Events detected	Net counting time (hours)	Accumulated Pt$^-$ charge (mC)[a]	Abundance relative to Pt
^{288}Ds	0	1.85	208	$<2 \times 10^{-15}$
^{289}Ds	0	1.85	208	$<2 \times 10^{-15}$
^{290}Ds	0	1.85	208	$<2 \times 10^{-15}$
^{291}Ds	0	1.85	208	$<2 \times 10^{-15}$
^{292}Ds	0	4.14	435	$<9 \times 10^{-16}$
^{293}Ds	0	4.14	435	$<9 \times 10^{-16}$
^{294}Ds	0	4.14	435	$<9 \times 10^{-16}$
^{295}Ds	0	4.14	435	$<9 \times 10^{-16}$

[a]To obtain the accumulated charge, the measured Pt$^-$ current was normalized to the time period where the respective Ds isotopes were collected (1 mC = 6.25×10^{15} ions).

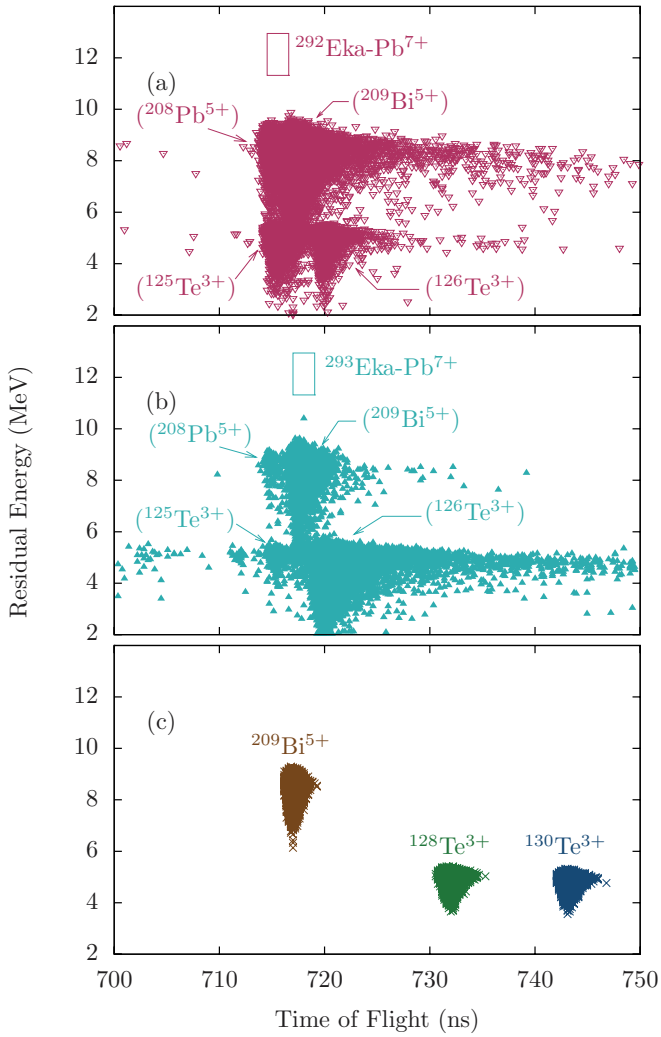

FIG. 8. (Color online) E_{res} vs TOF spectra for (a) ^{292}Eka-Pb^{7+}, (b) ^{293}Eka-Pb^{7+}, and (c) reference ions, plotted in the same way as described in the caption of Fig. 4. These spectra were accumulated during the second beam time of the Eka-Pb measurement. No event was captured within the SHE windows. Intense background peaks of ^{209}Bi^{5+}, ^{208}Pb^{5+}, ^{126}Te^{3+}, and ^{125}Te^{3+} can be seen in both the spectrum of the ^{292}Eka-Pb^{7+} and ^{293}Eka-Pb^{7+} setups.

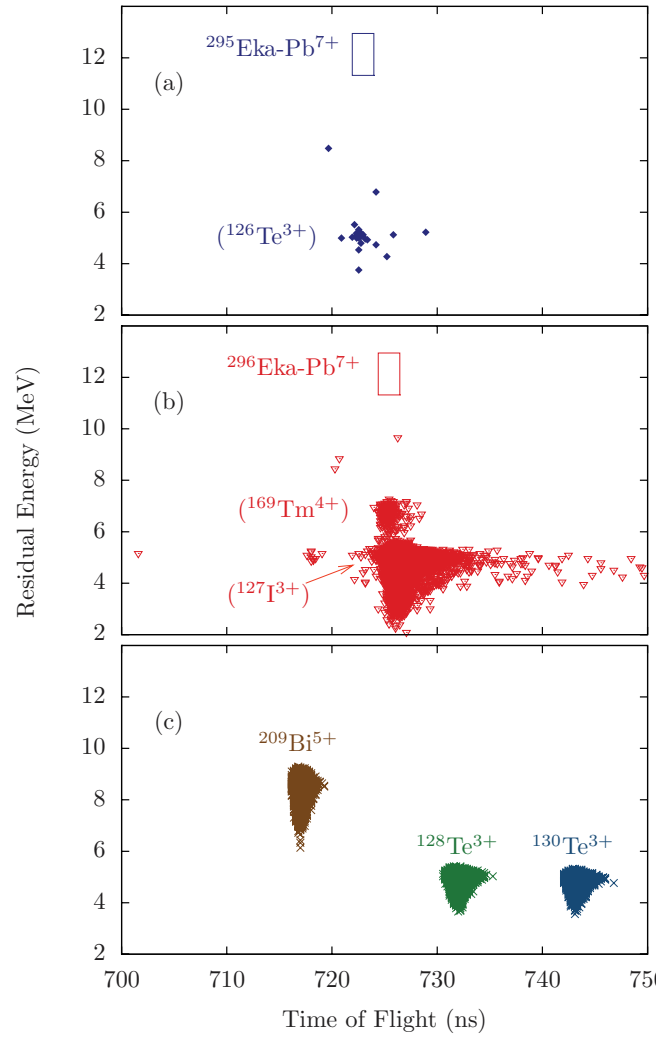

FIG. 9. (Color online) E_{res} vs TOF spectra for (a) ^{295}Eka-Pb^{7+}, (b) ^{296}Eka-Pb^{7+}, and (c) reference ions, plotted in the same way as described in the caption of Fig. 4. These spectra were accumulated during the first beam time of the Eka-Pb measurement. Whereas in the spectrum for ^{295}Eka-Pb^{7+} only a few events of ^{126}Te^{3+} were detected, the spectrum for ^{296}Eka-Pb^{7+} contains intense background peaks of ^{169}Tm^{4+} and ^{127}I^{3+}.

intensities. Although the background count rates in these two setups were the most intense of all measured Eka-Pb setups, the level of pileup was not excessive. Not a single event was detected within the windows for the superheavy ion species.

The composite spectrum of all runs on ^{295}Eka-Pb^{7+} and ^{296}Eka-Pb^{7+} measured in the first beam time is shown in Fig. 9. In the setup of ^{295}Eka-Pb^{7+} a few events of ^{126}Te^{3+} could be identified, whereas well-defined peaks of ^{127}I^{3+} and ^{169}Tm^{4+} were detected in the ^{296}Eka-Pb^{7+} setup. The windows for ^{295}Eka-Pb^{7+} and ^{296}Eka-Pb^{7+} remained empty.

Figure 10 presents the E_{res} vs TOF spectra for the ^{297}Eka-Pb^{7+} and ^{299}Eka-Pb^{7+} accumulated during the first beam time, which is also representative for the remeasured spectrum of the second beam time. Again the windows of the superheavy species were free of events. Background peaks of ^{85}Rb^{2+} and ^{170}Er^{4+} for the ^{297}Eka-Pb^{7+} setup, and ^{128}Te^{3+} and ^{171}Yb^{4+} for the ^{299}Eka-Pb^{7+} setup were identified, respectively. In Table VI the key data of the Eka-Pb measurements are listed.

The last part of this study was addressed to the search for ^{A}Eka-Bi (A = 293–300) in natural bismite and chemically purified Bi samples. In the first beam time on July 1–2, 2009, a total of 38 runs were performed to search for ^{293}Eka-Bi, ^{294}Eka-Bi, ^{295}Eka-Bi, and ^{296}Eka-Bi in the 7+ charge state. Figures 11 and 12 show the associated E_{res} vs TOF spectra accumulated during the first beam time. In the setup for ^{293}Eka-Bi^{7+} [Fig. 11(a)] obviously the ^{209}Bi fragment of an unknown molecule with $m \sim 293$ was detected, which could pass the high-energy side of VERA nearly unsuppressed, due to the close-lying m/q ratio. The heavy background generated a belt of pileup events [light symbols in Fig. 11(a)] which reached the window for ^{293}Eka-Bi^{7+}. Applying the pulse-width criterion explained in Fig. 7 of Dellinger *et al.* [18], the

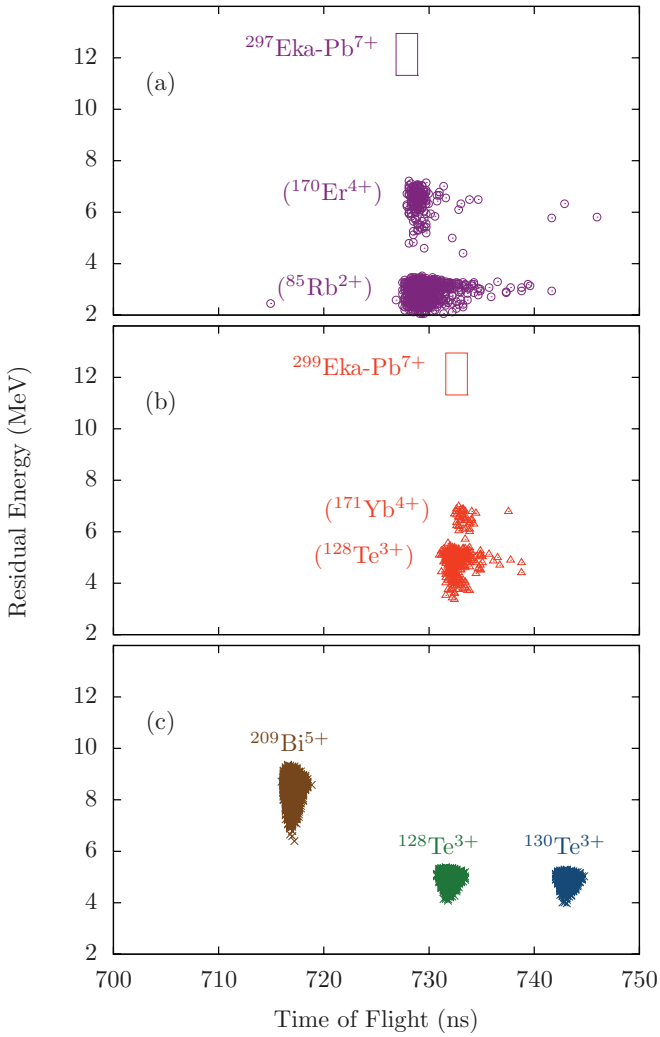

FIG. 10. (Color online) E_{res} vs TOF spectra for (a) ^{297}Eka-Pb^{7+}, (b) ^{299}Eka-Pb^{7+}, and (c) reference ions, plotted in the same way as described in the caption of Fig. 4. Whereas the search for the isotopes ^{297}Eka-Pb and ^{299}Eka-Pb was performed in both Eka-Pb beam times, only the events accumulated in the first beam time are shown above. In the ^{297}Eka-Pb^{7+} setup background peaks of ^{170}Er^{4+} and ^{85}Rb^{2+} of moderate intensity were recorded. In the ^{299}Eka-Pb^{7+} setup the peaks of ^{171}Yb^{4+} and ^{128}Te^{3+} were observed. Not a single event was detected in one of the SHE windows.

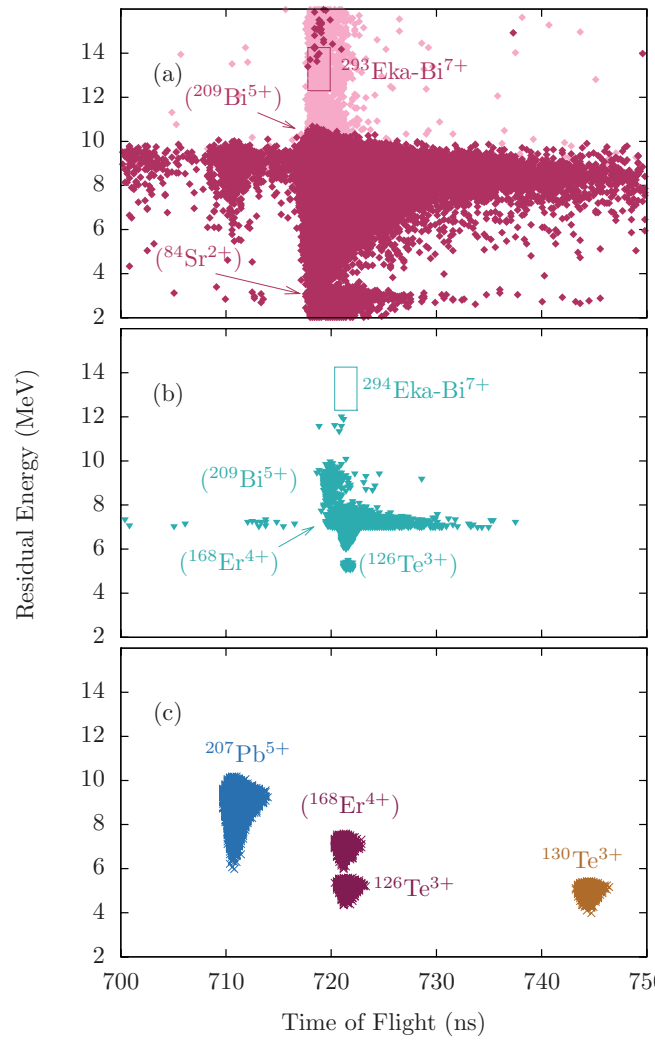

FIG. 11. (Color online) E_{res} vs TOF spectra for (a) ^{293}Eka-Bi^{7+}, (b) ^{294}Eka-Bi^{7+}, and (c) reference ions, plotted in the same way as described in the caption of Fig. 4. These spectra were recorded during the first beam time of the Eka-Bi measurement. The very strong background of ^{209}Bi^{5+} in the setup for ^{293}Eka-Bi^{7+} generated an intense belt of pileup events covering the window for ^{293}Eka-Bi^{7+}. However, the additional pulse-width criterion could reject most of these events. Only six events resisted all filters applied in the evaluation process. In spectrum (b), related to ^{294}Eka-Bi^{7+}, three background peaks could be identified: ^{209}Bi^{5+}, ^{168}Er^{4+}, and ^{126}Te^{3+}. Below a residual energy of 7 MeV only channels containing more than 50 events are plotted to point out the peak position of ^{126}Te^{3+}.

TABLE VI. Results of the AMS search for superheavy Eka-Pb isotopes in galena.

Rare isotope	Events detected	Net counting time (hours)	Accumulated PbF_3^- charge (mC)	Abundance relative to Pb
^{292}Eka-Pb	0	3.60	4.6	$<6 \times 10^{-14}$
^{293}Eka-Pb	0	3.64	5.0	$<6 \times 10^{-14}$
^{295}Eka-Pb	0	2.44	7.5	$<4 \times 10^{-14}$
^{296}Eka-Pb	0	2.45	6.5	$<4 \times 10^{-14}$
^{297}Eka-Pb	0	6.06	11.5	$<3 \times 10^{-14}$
^{299}Eka-Pb	0	6.06	12.2	$<2 \times 10^{-14}$

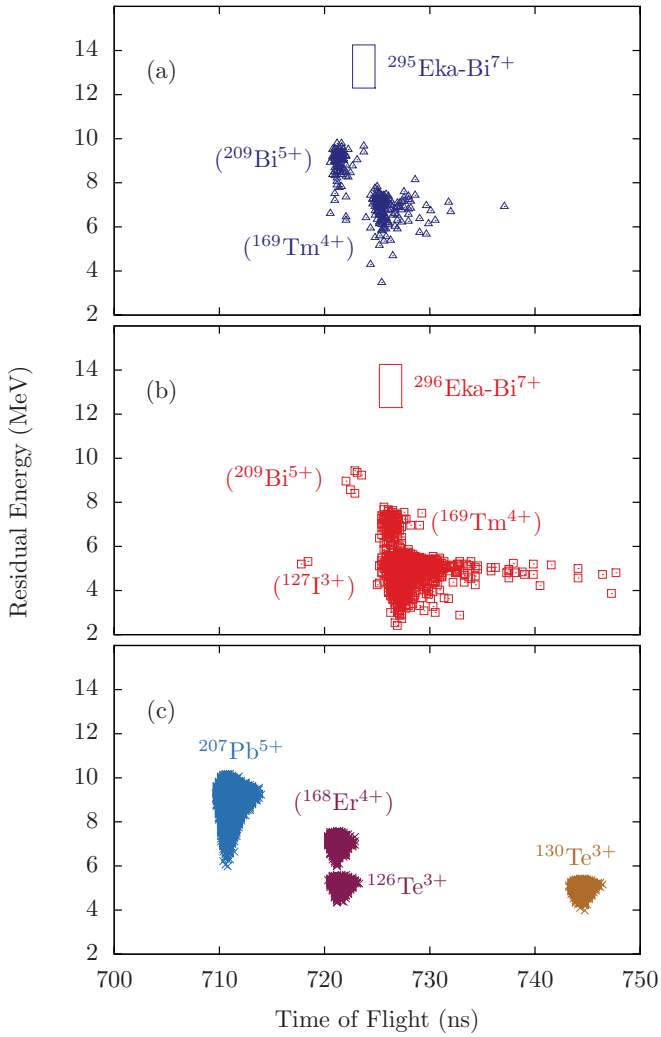

FIG. 12. (Color online) E_{res} vs TOF spectra for (a) ^{295}Eka-Bi^{7+}, (b) ^{296}Eka-Bi^{7+}, and (c) reference ions, plotted in the same way as described in the caption of Fig. 4. These spectra were recorded during the first beam time of the Eka-Bi measurement. In both SHE windows not a single event was detected. Whereas decent peaks of ^{209}Bi^{5+} and ^{169}Tm^{4+} form the background in the setup for ^{295}Eka-Bi^{7+}, an intense peak of the ^{127}I^{3+} was additionally detected in the setup for ^{296}Eka-Bi^{7+}.

bulk of pileup events could be excluded, leaving only six events [dark symbols in Fig. 11(a)] within the window for ^{293}Eka-Bi^{7+}. Since the means of background rejection are exhausted by combining all three measured parameters (E_{res}, TOF, and pulse width), the six events had to be treated as real events in our calculation of atomic ratios. However, the pulse-width discrimination against pileup is less effective if the sum of background events happen to produce energy peaks with widths similar to those expected for ^{293}Eka-Bi^{7+} ions (see Fig. 13). In addition, the "good" events within the window cluster in the upper left-hand corner, which one would not expect for SHE events. The background in the spectrum for ^{294}Eka-Bi^{7+} [Fig. 11(b)] appeared comparably moderate: The peaks of ^{126}Te^{3+}, ^{168}Er^{4+}, and again ^{209}Bi^{5+} could be identified. The window for ^{294}Eka-Bi^{7+} remained clean.

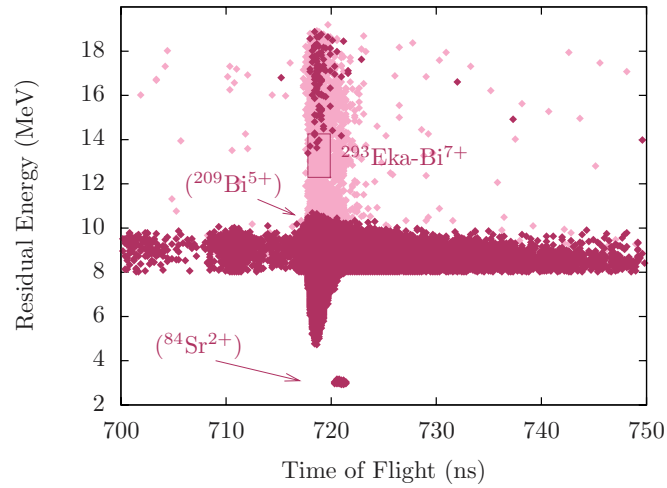

FIG. 13. (Color online) Expanded-energy view of Fig. 11(a), displaying the full-energy pileup events from the strong ^{209}Bi^{5+} background. To check for possible lower-energy background peaks, only channels with more than 30 counts are displayed below 8 MeV residual energy. Besides ^{84}Sr^{2+} ions, no other background seems to be present. The rest of the background is dominated by the strong ^{209}Bi^{5+} peak. The distribution of events after the pulse-width criterion was applied (dark symbols) indicates that the rejection is less effective the closer to the full-energy pileup one gets, because the pulse width decreases with increasing pileup pulse height (for details see Fig. 7 of Ref. [18]). The six events remaining in the ^{293}Eka–Bi^{7+} window after pulse-width suppression—from a total of 346—are not centered in the window, which makes it highly unlikely that they are real ^{293}Eka-Bi events.

Neither in the spectrum of ^{295}Eka-Bi^{7+} [Fig. 12(a)] nor in that of ^{296}Eka-Bi^{7+} [Fig. 12(b)] was any event detected within the superheavy window. The relatively small peaks of ^{169}Tm^{4+} and ^{209}Bi^{5+} in Fig. 12(a) indicate a small background count rate, whereas an additional, more intense peak of ^{127}I^{3+} is seen in Fig. 12(b).

In the 43 runs of the second beam time on July 2–3, 2009, the AMS system was tuned for ^{297}Eka-Bi, ^{298}Eka-Bi, ^{299}Eka-Bi, and ^{300}Eka-Bi in the 7+ charge state. Figure 14 shows the E_{res} vs TOF spectra for ^{297}Eka-Bi^{7+} [Fig. 14(a)] and ^{298}Eka-Bi^{7+} [Fig. 14(b)]. In both spectra the window for the superheavy species are free of events. The background of ^{85}Rb^{2+} and ^{170}Er^{4+} for the ^{297}Eka-Bi^{7+} setup and ^{128}Te^{3+} for the ^{298}Eka-Bi^{7+} setup did not produce pileup events. Similar results were found for ^{299}Eka-Bi^{7+} and ^{300}Eka-Bi^{7+} [Figs. 15(a) and 15(b)]. No event was detected within the windows for the rare ions, and only a moderate background of ^{171}Yb^{4+} was found in the setup for ^{299}Eka-Bi^{7+} and of ^{86}Sr^{2+} in the setup of ^{300}Eka-Bi^{7+}, respectively.

Unfortunately, there was no current measured during the first beam time which could be used for normalization of the detected events. Therefore in column 5 of Table VII only estimated values for the abundance of ^{293}Eka-Bi, ^{294}Eka-Bi, ^{295}Eka-Bi, and ^{296}Eka-Bi relative to ^{209}Bi can be given, based on the high-energy current of ^{209}Bi^{5+} measured during the second beam time. In column 4 of Table VII the (calculated) ionic charge accumulated in the high-energy Faraday cup for

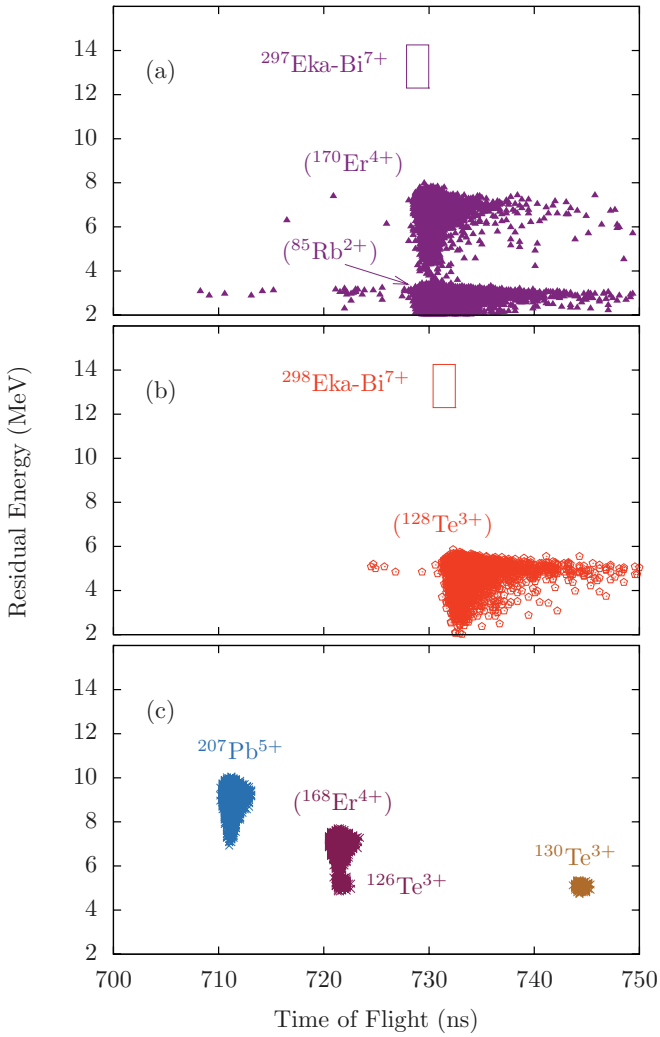

FIG. 14. (Color online) E_{res} vs TOF spectra for (a) ^{297}Eka-Bi^{7+}, (b) ^{298}Eka-Bi^{7+}, and (c) reference ions, plotted in the same way as described in the caption of Fig. 4. These spectra were recorded during the second beam time of the Eka-Bi measurement. The background in the ^{297}Eka-Bi^{7+} setup consisted of the peaks of ^{170}Er^{4+} and ^{85}Rb^{2+}. In the setup for ^{298}Eka-Bi^{7+} only background events of ^{128}Te^{3+} were detected. Not a single event was detected in the windows of ^{297}Eka-Bi^{7+} and ^{298}Eka-Bi^{7+}.

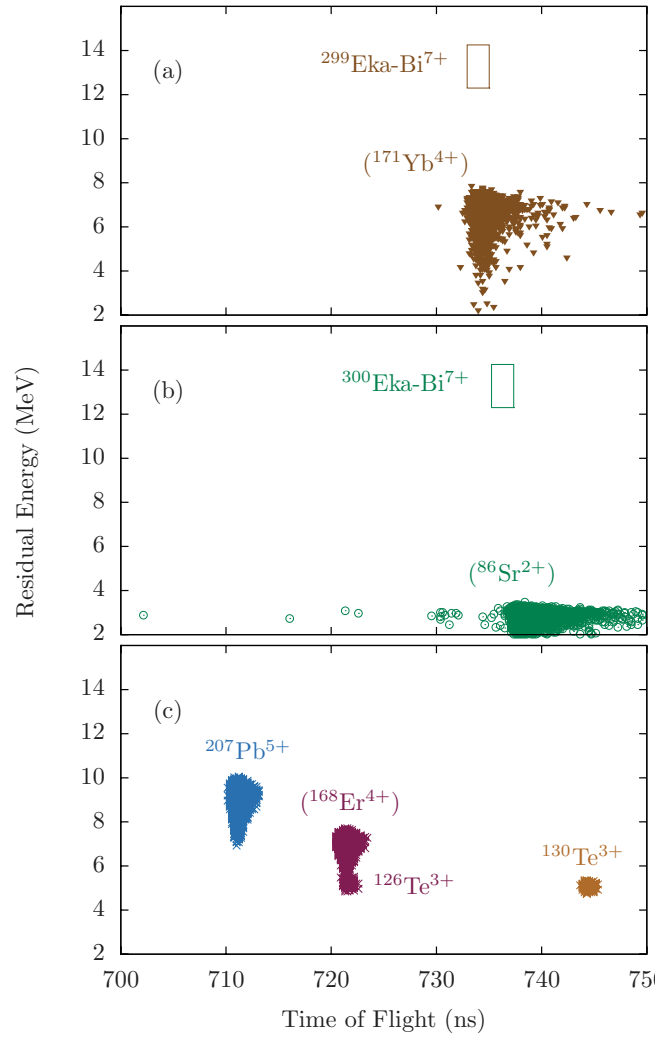

FIG. 15. (Color online) E_{res} vs TOF spectra for (a) ^{299}Eka-Bi^{7+}, (b) ^{300}Eka-Bi^{7+}, and (c) reference ions, plotted in the same way as described in the caption of Fig. 4. These spectra were recorded during the second beam time of the Eka-Bi measurement. Only the background peaks of ^{171}Yb^{4+} and ^{86}Sr^{2+} were found in the setups for ^{299}Eka-Bi^{7+} and ^{300}Eka-Bi^{7+}, respectively. The windows for the SHE isotopes remained empty.

the respective setups is listed. The values denote again an estimate based on the average currents of the second beam time and the measurement duration of the first beam time.

Based on early calculation of the production rates for SHEs in the nuclear *r* process [8], the results of our measurements allow to deduce an upper limit for the total half-lives of the investigated superheavy nuclides. Assuming a rather optimistic production ratio of the superheavy nuclide ^{294}Ds relative to Pt of ^{294}Ds/Pt = 0.03 [8], the measured upper limit for the present abundance of 9×10^{-16} relative to natural Pt implies an upper limit for the total half-life of ∼100 million years. It has to be emphasized that an uncertainty of a factor of 2 in the measured abundance ratio would increase the half-life only marginally by 2 million years. Production ratios of ^{291}Ds/Pt∼0.13 and ^{292}Ds/Pt∼0.07 [8] combined with the abundance limits of these respective nuclides determined in this study (see Table V) lead to upper limits for the half-lives of 97 and 99 million years, respectively. For ^{293}Rg, investigated in our previous study [18], a ^{293}Rg/^{197}Au limit of 5×10^{-16} was found. Since the Au/Pt abundance ratio in the solar system is ∼0.144 [43], a production ratio of ^{293}Rg/^{197}Au of 0.76 is deduced from the ^{293}Rg/Pt abundance of 0.109 [8]. This then leads to an upper limit for the half-life of ^{293}Rg of 90 million years.

More recent calculations of possible *r*-process scenarios, e.g., Panov *et al.* [15] for neutron star mergers, show relative production ratios of SHE/Pt which are many orders of magnitude smaller than those of Schramm and Fowler [8] used for the half-life estimates above. Such a dramatic reduction of the production ratio immediately leads to half-lives for the SHEs in the range of several hundred million years to be detectable at all. However, due to the exceptional selectivity

TABLE VII. Results of the AMS search for superheavy Eka-Bi isotopes in natural bismite and commercial Bi powder.

Rare isotope	Events detected	Net counting time (hours)	$^{209}Bi^{5+}$ ions accumulated in the high-energy Faraday cup[a]	Abundance relative to Bi
^{293}Eka-Bi	6[b]	1.48	6.5×10^{13}	$<3 \times 10^{-12}$
^{294}Eka-Bi	0	1.74	7.7×10^{13}	$<5 \times 10^{-13}$
^{295}Eka-Bi	0	1.74	7.7×10^{13}	$<5 \times 10^{-13}$
^{296}Eka-Bi	0	1.74	7.7×10^{13}	$<5 \times 10^{-13}$
^{297}Eka-Bi	0	2.23	9.8×10^{13}	$<5 \times 10^{-13}$
^{298}Eka-Bi	0	2.23	9.8×10^{13}	$<5 \times 10^{-13}$
^{299}Eka-Bi	0	2.23	9.8×10^{13}	$<5 \times 10^{-13}$
^{300}Eka-Bi	0	2.23	9.8×10^{13}	$<5 \times 10^{-13}$

[a]To obtain the accumulated ion number, the measured $^{209}Bi^{5+}$ current was normalized to the time period where the respective Ds isotopes were collected.

[b]As discussed in the text and in the caption of Fig. 13, these six events are most likely not real ^{293}Eka-Bi events. However, because they cannot be firmly excluded, the upper limit in column 5 is higher than for those isotopes where no events were observed.

of AMS, this measurement technique again would be "the method of choice."

Nevertheless, it should be pointed out that one cannot completely exclude possible loopholes in our discussion that would lead to negative results for the detection of SHEs with AMS. (1) SHEs must be produced in the *r* process. An early cutoff in the *r* process as discussed by Howard and Nix [44] may result in the absence of SHEs in nature. (2) The half-life of the SHE species must be at least in the range of 100 million years in order to make them detectable with AMS. (3) The chemical behavior should not differ from the properties of the sample material investigated, in order to follow these materials since the condensation of matter in the early solar system. (4) The EA of the SHEs must be positive to be able to form negative ions in the sputter source of the AMS system. It seems that (1) and (2) are the most uncertain assumptions. Assumption (3) may not be such a severe condition, since calculations show [45] that there should be "no striking chemical differences between platinum and darmstadtium." In addition, the AMS measurement of a particular SHE nuclide accepts neighboring isobars as well (which means also neighboring elements), as already pointed out in Sec. I. The production of negative ions (4) should actually be quite feasible, as exemplified by the estimates of electron affinities for SHEs in Table II.

V. CONCLUSION

The recent searches for superheavy elements in nature with AMS [16–18] were triggered by the intriguing results of positive evidence for SHEs in the 10^{-10}–10^{-12} abundance range, found in the inductively coupled plasma sector field mass spectrometry (ICP-SFMS) measurements of Marinov *et al.* [46–48]. Neither the results of neutron-deficient thorium isotopes were confirmed with AMS [16,17], nor the claim for a SHE nuclide with $A = 292$ in thorium [17] and for neutron-deficient Rg isotopes in gold [18]. The AMS results set upper limits of abundances, which were several orders of magnitudes lower than the positive findings of the Marinov group. Although it is difficult to judge other group's experiments, we are forced to conclude that unknown artifacts may have affected the ICP-SFMS measurements at this unusually low abundance level for this technique.

In addition to the four neutron-deficient thorium isotopes and a possible ^{292}Eka-Th nuclide [17], and the two neutron-deficient Rg isotopes [18], our results on 30 SHE nuclides in the mass range $A = 288$–300 in the vicinity of the center of the island of stability [49] set upper limits for the existence of these nuclides in natural Au [18], Pt, Pb, and Bi, which can hardly be met by any other technique. Although our results make it unlikely that long-lived SHE nuclides do exist, the continuous improvement of the AMS technique will allow one to search ever deeper into this largely unexplored territory of the chart of nuclides. And perhaps, one day, a small island of stability will appear fortuitously in the vast sea of instability.

ACKNOWLEDGMENT

We thank Dr. Uwe Kolitsch of the Department of Mineralogy and Petrology of the Natural History Museum Vienna, for the donation of sample material used in this study.

[1] W. D. Myers and W. J. Swiatecki, Nucl. Phys. **81**, 1 (1966).
[2] S. G. Nilsson, J. R. Nix, A. Sobiczewski, Z. Szymanski, S. Wycech, C. Gustafson, and P. Möller, Nucl. Phys. A **115**, 545 (1968).
[3] V. M. Strutinsky, Nucl. Phys. A **122**, 1 (1968).
[4] S. G. Nilsson, C. F. Tang, A. Sobiczewski, Z. Szymanski, S. Wycech, C. Gustafson, I.-L. Lamm, P. Möller, and B. Nilsson, Nucl. Phys. A **131**, 1 (1969).
[5] G. Herrmann, Nature (London) **280**, 543 (1979).

[6] G. N. Flerov and G. M. Ter-Akopian, Rep. Prog. Phys. **46**, 817 (1983).
[7] E. O. Fiset and J. R. Nix, Nucl. Phys. A **193**, 647 (1972).
[8] D. N. Schramm and W. A. Fowler, Nature (London) **231**, 103 (1971).
[9] K. A. Brueckner, J. H. Chirico, S. Jorna, H. W. Meldner, D. N. Schramm, and P. A. Seeger, Phys. Rev. C **7**, 2123 (1973).
[10] W. Stephens, J. Klein, and R. Zurmühle, Phys. Rev. C **21**, 1664 (1980).
[11] S. Nozette and W. V. Boynton, Science **214**, 331 (1981).
[12] D. C. Hoffman, F. O. Lawrence, J. L. Mewherter, and F. M. Rourke, Nature (London) **234**, 132 (1971).
[13] N. Kinoshita *et al.*, J. Phys. G **35**, 014033 (2008).
[14] B. A. Buchholz, S. R. Biegalski, S. M. Whitney, S. J. Tumey, and C. J. Weaver, Nucl. Instrum. Methods B **268**, 773 (2010).
[15] I. V. Panov, I. Yu. Korneev, and F.-K. Thielemann, Phys. At. Nucl. **72**, 1026 (2009).
[16] L. Lachner, I. Dillmann, T. Faestermann, G. Korschinek, M. Poutivtsev, and G. Rugel, Phys. Rev. C **78**, 064313 (2008).
[17] F. Dellinger, O. Forstner, R. Golser, W. Kutschera, A. Priller, P. Steier, A. Wallner, and G. Winkler, Nucl. Instrum. Methods B **268**, 1287 (2010).
[18] F. Dellinger, W. Kutschera, O. Forstner, R. Golser, A. Priller, P. Steier, A. Wallner, and G. Winkler, Phys. Rev. C **83**, 015801 (2011).
[19] M. Stoyer, Nature (London) **442**, 876 (2006).
[20] J. C. Rienstra-Kiracofe, G. S. Tschumper, and H. F. Schaefer III, Chem. Rev. **102**, 231 (2002).
[21] R. Middleton, "A negative-ion cookbook," University of Pennsylvania, 1990 [http://www.pelletron.com/cookbook.pdf].
[22] E. Eliav, U. Kaldor, P. Schwerdtfeger, B. A. Hess, and Y. Ishikawa, Phys. Rev. Lett. **73**, 3203 (1994).
[23] M. Seth, K. Faegri, and P. Schwerdtfeger, Angew. Chem. Int. Ed. **37**, 2493 (1998).
[24] K. T. Giju, F. De Proft, and P. Geerlings, J. Phys. Chem. A **109**, 2925 (2005).
[25] S. L. Bennett, J. Ling-Fai Wang, J. L. Margrave, and J. L. Franklin, High Temp. Sci. **7**, 142 (1975).
[26] E. Eliav, U. Kaldor, and Y. Ishikawa, Mol. Phys. **94**, 181 (1998)
[27] C. Vockenhuber, I. Ahmad, R. Golser, W. Kutschera, V. Lichtenstein, A. Priller, P. Steier, and S. Winkler, Int. J. Mass Spectrom. **223-224**, 713 (2003).
[28] P. Steier, R. Golser, W. Kutschera, A. Priller, C. Vockenhuber, and S. Winkler, Nucl. Instrum. Methods **223-224**, 67 (2004).
[29] G. T. Seaborg and J. L. Bloom, Sci. Am. **220/4**, 57 (1969).
[30] G. T. Seaborg, J. Chem. Educ. **46**, 626 (1969).
[31] S. Hofmann, Physics **3**, 31 (2010).
[32] A. Türler, J. Nucl. Radiochem. Sci. **5**, R19 (2004).
[33] M. Schädel *et al.*, Nature (London) **388**, 55 (1997).
[34] R. Eichler *et al.*, Nature (London) **407**, 63 (2000).
[35] Ch. Düllmann *et al.*, Nature (London) **418**, 859 (2002).
[36] R. Eichler *et al.*, Nature (London) **447**, 72 (2007).
[37] J. A. Ferry, Nucl. Instrum. Methods A **328**, 28 (1993).
[38] J. Southon and G. M. Santos, Nucl. Instrum. Methods B **259**, 88 (2007).
[39] P. Steier (private communication).
[40] E. Hrnecek, P. Steier, and A. Wallner, Appl. Radiat. Isot. **63**, 633 (2005).
[41] E. Hrnecek, R. Jakopič, A. Wallner, and P. Steier, J. Radioanal. Nucl. Chem. **276**, 789 (2008).
[42] G. J. Feldman, and R. D. Cousins, Phys. Rev. D **57**, 3873 (1998).
[43] A. G. W. Cameron, Space Sci. Rev. **15**, 121 (1970).
[44] W. M. Howard and J. R. Nix, Nature (London) **247**, 17 (1974).
[45] M. Patzschke and P. Pyykkö, Chem. Commun. **17**, 1982 (2004)
[46] A. Marinov, I. Rodushkin, Y. Kashiv, L. Halicz, I. Segal, A. Pape, R. V. Gentry, H. W. Miller, D. Kolb, and R. Brandt, Phys. Rev. C **76**, 021303(R) (2007).
[47] A. Marinov, I. Rodushkin, A. Pape, Y. Kashiv, D. Kolb, R. Brandt, R. V. Gentry, H. W. Miller, L. Halicz, and I. Segal, Int. J. Mod. Phys. E **18**, 621 (2009).
[48] A. Marinov, I. Rodushkin, D. Kolb, A. Pape, Y. Kashiv, R. Brandt, R. V. Gentry, and H. W. Miller, Int. J. Mod. Phys. E **19**, 131 (2010).
[49] A. Sobiczewski and K. Pomorski, Prog. Part. Nucl. Phys. **58**, 292 (2007).